

# The Use of Schwarz-Christoffel Transformations in Determining Acoustic Resonances

Colleen B. Lanz

Thesis submitted to the Faculty of the  
Virginia Polytechnic Institute and State University  
in partial fulfillment of the requirements for the degree of

Master of Science  
in  
Mathematics

Robert C. Rogers, Chair  
Jeff Borggaard  
Tao Lin

July 6, 2010  
Blacksburg, Virginia

Keywords: Schwarz-Christoffel Transformations, Polygons, Eigenvalues, Laplacian

# The Use of Schwarz-Christoffel Transformations in Determining Acoustic Resonances

Colleen Lanz

(ABSTRACT)

In this thesis, we set out to provide an enhanced set of techniques for determining the eigenvalues of the Laplacian in polygonal domains. Currently, finite-element methods provide a numerical means by which we can approximate these eigenvalues with ease. However, we would like a more analytic method which may allow us to avoid a basic parameter sweep in finite-element software such as COMSOL to determine what could possibly be an “optimal” distribution of eigenvalues. The hope is that this would allow us to draw conclusions about the acoustic quality of a pentagonally-shaped room. First, we find the eigenvalues using a common finite-element method through COMSOL Multiphysics. We then examine another method which makes use of conformal maps and Schwarz-Christoffel transformations with the prospect that it might provide a more analytic understanding of the calculation of these eigenvalues and possibly allow for variation of certain parameters. This method, as far as we could find, had not yet been developed on the pentagon. We end up carrying this method through nearly all of the steps necessary in finding these eigenvalues. We find that the finite-element method is not only easier to use, but is also more efficient in terms of computing power.

# Contents

<b>1</b>	<b>Introduction</b>	<b>1</b>
<b>2</b>	<b>Sound Waves</b>	<b>3</b>
2.1	Definition of Sound . . . . .	3
2.2	The Significance of Room Modes . . . . .	3
<b>3</b>	<b>Derivation of the 3-Dimensional Wave Equation with Boundary Conditions</b>	<b>6</b>
<b>4</b>	<b>Solution by Generalized Separation of Variables</b>	<b>9</b>
<b>5</b>	<b>Determining the Modes for a Rectangular Room</b>	<b>11</b>
<b>6</b>	<b>The Acoustic Disadvantages of Constructing Rectangular Rooms</b>	<b>14</b>
<b>7</b>	<b>The Acoustic and Constructional Advantages of Pentagonal Rooms</b>	<b>15</b>
<b>8</b>	<b>Finite Element Methods for Solving the PDE</b>	<b>16</b>
<b>9</b>	<b>Finding Eigenvalues Using Schwarz-Christoffel Transformations</b>	<b>22</b>
9.1	Cureton and Kuttler’s Method . . . . .	22
9.2	Conformal Maps . . . . .	23
9.3	Introduction to the Schwarz-Christoffel Transformation . . . . .	24
9.4	The Rayleigh-Ritz Method . . . . .	29
9.4.1	“Intuitive” Explanations of the Rayleigh-Ritz Theorems . . . . .	30

9.4.2	Rayleigh Quotient in Cureton and Kuttler . . . . .	31
9.5	Calculating the Integrals . . . . .	31
9.6	Calculating $I_{00}$ . . . . .	33
9.7	Implementation of the Method Using $I_{00}$ . . . . .	34
<b>10</b>	<b>Results</b>	<b>36</b>
10.1	Observations about $I_{00}$ . . . . .	36
<b>11</b>	<b>Conclusion</b>	<b>39</b>

# List of Figures

8.1	The contour map of the eigenfunctions associated with the first eigenvalue in COMSOL. . . . .	18
8.2	The contour map of the eigenfunctions associated with the third eigenvalue in COMSOL. . . . .	19
8.3	The contour map of the eigenfunctions associated with the fifth eigenvalue in COMSOL. . . . .	19
8.4	The contour map of the eigenfunctions associated with the sixteenth eigenvalue in COMSOL. . . . .	20
8.5	Using COMSOL with MATLAB, a triangulated mesh is formulated on the regular pentagon with unit sides. . . . .	20
8.6	The eigenvalues of each of these symmetries were calculated separately in the Cureton and Kuttler paper. . . . .	21
9.1	Conformal maps preserve angles and sense (direction). . . . .	23
9.2	The Schwarz-Christoffel Transformation maps the $x$ -axis to some closed polygon in $w$ . . . . .	24
9.3	The transformation takes the tangent, $t$ , of the curve $C$ in the $z$ plane to the tangent, $\tau$ of the curve $\Gamma$ in the $w$ plane. . . . .	25
9.4	As $z$ traverses the $x$ -axis, the Schwarz-Christoffel Transformation causes it to make abrupt changes in direction in the $w$ plane as it passes each $x_i$ in the $z$ plane. . . . .	26
9.5	For each $x_i$ crossed by $z$ in the $z$ -plane, a turn of $\pi - \alpha_i$ occurs in the $w$ -plane.	26
9.6	We would like to determine a function which takes figure 9.6a to figure 9.6b.	27
9.7	We would like to determine a function which takes Figure 9.7a, the upper half plane, to Figure 9.7b, a polygon with right angles. . . . .	28

9.8	Three points on the $x$ -axis of the $z$ plane get mapped to an equilateral triangle in the $w$ plane with side length $b$ . . . . .	29
9.9	$\ln(A_n(r))$ for $n = 0, 1, 2, 3, 4$ and $n = 17, 18, 19, 20, 21$ . . . . .	32
9.10	The first figure is $J_0(j_{0,10}r)$ versus $r$ and the second is $J_0(j_{0,100}r)$ . . . . .	33

# List of Tables

8.1	Comparison of the eigenvalues of the unit-sided hexagon in the Cureton and Kuttler paper with those found using finite-element software. . . . .	17
8.2	The first sixteen eigenvalues of the unit-sided pentagon found using finite-element software. . . . .	18
9.1	The Rayleigh-Ritz array which shows how the method is used to find closer approximations of the eigenvalues. . . . .	30
10.1	A comparison of the calculation of integrals using the iterative $I_{00}$ algorithm and MATLAB's direct quadrature. . . . .	38

# Chapter 1

## Introduction

In this paper, we discuss two methods for finding the eigenvalues of the Laplacian on two-dimensional geometries. The first method is one that is commonly used today and uses finite-element methods with an easy-to-use interface (like that of COMSOL) to numerically approximate the eigenvalues. The second method is the one that will be inspected more deeply. It utilizes conformal maps and Schwarz-Christoffel transformations like those developed by Toby Driscoll to find these same eigenvalues (Driscoll 169-172). The benefit of this latter method is its potential to be more analytic in nature.

Some theory has previously been developed for this Schwarz-Christoffel transformation method, but has not been employed on the regular pentagon, which, as we see, is the geometry of choice for this paper.

As we discuss in more detail later, we find only partial success with this transformation method. In particular, the numerical experiments were more difficult to perform and had substantially higher computational time than standard FEM eigenvalue methods. Furthermore, while some aspects of the method are analytic, the Schwarz-Christoffel transformations did not make for easy analysis of the final results, as was originally hoped. Additionally, we were unable to accurately calculate the eigenvalues using this method although we managed to implement many of the practices currently used for Schwarz-Christoffel transformations.

One application of finding these eigenvalues can be found in the world of acoustics. In particular, the goal of this thesis is to inspect the acoustic properties of a pentagonally-shaped room. Rooms with these geometry are often constructed by sound engineers because it is both relatively easy to build and produces significant acoustic advantages, as we will see.

The remainder of the paper is laid out as follows. In Chapter 2, we look into the physics of sound and why inspection of the room modes are of acoustic importance. In Chapter 3, we derive the three-dimensional wave equation which provides the motivation for the use of the Laplacian in our eigenvalue problem. In Chapters 4 and 5, we solve the wave equation and



use this solution to find the modes for the case of a rectangular room. Then we see why we need to expand our scope to include rooms that are not rectangular in Chapter 6. We also see why, instead, we should focus our attention on pentagonally-shaped rooms, as is discussed in Chapter 7. In Chapter 8, we see the results from the computation of the eigenvalue problem by finite-element methods. Finally, in Chapter 9, we get into the mathematical details of this alternate method of solving the eigenvalue problem. Chapter 10 contains some of the results from these numerical experiments.

# Chapter 2

## Sound Waves

### 2.1 Definition of Sound

Sound, as it is received by the ear, is simply a longitudinal wave caused by changes in air pressure. One can think of one such a wave as a long spring that has been jolted forward on one end, causing a pulse along the spring. As the energy of the pulse propagates along the spring, some parts of the spring compress while others spread out. The dense section of the spring, caused by the energy from the pulse, is called a **compression**. The sparser sections are called **rarefactions**.

The same principle holds with air particles. When a noise is produced, energy is propagated through these particles, causing minute changes in air pressure. Each cubic inch of air contains more than a million air molecules (Everest 7). The human ear is incredibly sensitive to changes in pressure. The faintest sound that can be heard corresponds to a variation in pressure of  $20 \mu\text{Pascal}$ , which is approximately 5,000 times smaller than atmospheric pressure (Everest 9).

### 2.2 The Significance of Room Modes

The boundaries (rigid walls) of the room in which the source is placed complicates the acoustics of the room considerably. Just as with reflections of light, when a sound wave is reflected on a plane surface, a new wave emanates from the surface as though it were being generated by an ‘image’ source behind the wall.

One of our main purposes here is to attempt to find the vibrational modes of different rooms, which are directly related to the eigenvalues of the Laplacian in the region. These modes

correspond to the natural resonances of the room. As we note below, engineers would like the resonant modes to be as evenly spaced as possible in order to accurately evaluate sounds produced within the room.

The shape of the room (in addition to materials covering the surface of the room) cause certain frequencies to reverberate longer and hence create louder sounds at these frequencies. The human ear, however, prefers a well-balanced signal at all frequencies.

In order to fully understand room modes and the role that they play in this eigenvalue problem, we must first discuss what is meant by **resonances** intuitively and why they are of particular interest to us. Let us suppose again, for simplicity, that we have a room with rectangular geometry. In yet another step of simplification, we can model the resonances of a rectangular room by considering a string, fixed at both ends.

Vibrations of a string of various frequencies behave much like sound waves in the air bouncing back and forth between the ends. Waves of certain frequencies create **standing waves**. They are the result of the superposition of two waves of the same frequency traveling in opposite directions. In order to create a **standing wave**, the **nodes** (points where the amplitude of the string is zero) and **antinodes** (the points of the highest amplitude of the string) must remain fixed. The first example (in which  $n = 1$ ) consists of having two nodes on the ends and one antinode in between. This is known as the **fundamental** or **first harmonic**. In this case, the wavelength,  $\lambda$ , is twice the length of the entire string,  $L$ :

$$\lambda_1 = 2L.$$

We can achieve the rest of the **harmonic series** of the standing wave by requiring that integer multiples of the wavelength must equal twice the length of the string:

$$\lambda_n = \frac{2L}{n}.$$

Our simple example of the string demonstrates that, just as there are certain frequencies which will resonate on the string based on the string's length, there are certain frequencies that will resonate in a room based on the room's shape and dimensions. This brings us to the concept of room modes.

**Room modes** are created by the interference of an original sound wave with its reflection off the walls of the room. For music engineers, they can often create problems with the lower frequency sounds, creating a “muddy” effect in the bass line because they emphasize some frequencies and mute others. Thus, the shape and construction of the mixing room is of the utmost importance when one is trying to most accurately replicate the true sound emitted from instruments. For example, in a rectangular room with width, length and height given by  $L_x$ ,  $L_y$  and  $L_z$ , respectively, the resonant frequencies,  $f$ , are given by

$$f = \left(\frac{c}{2}\right) \sqrt{\left(\frac{n_x}{L_x}\right)^2 + \left(\frac{n_y}{L_y}\right)^2 + \left(\frac{n_z}{L_z}\right)^2},$$

where  $n_x, n_y$  and  $n_z$  are integer room mode numbers and  $c$  is the speed of sound in air (roughly 344 m/s). We will see the derivation of this in Chapter 5.

In effect, the room modes will cause fluctuations (both positive and negative) in the amplitude (or volume) of the sound wave. Ideally, you want the room large enough or constructed in such a way as to allow the sound waves to naturally decay before interfering with their own reflections and distorting the original sound.

This interaction between the original wave and its reflection is a phenomenon referred to as **modal waves**. Sometimes, this interference will be constructive (resulting in a heightening of the amplitude) and other times, the interference will be destructive (resulting in reduction of the amplitude). Both types of interference are troublesome to sound engineers who want to replicate the original sound source as accurately as possible.

## Chapter 3

# Derivation of the 3-Dimensional Wave Equation with Boundary Conditions

Sound waves are simply disturbances in compressible gases. Recall the equations for conservation of mass and momentum in an inviscid gas (Billingham 36):

$$\frac{\partial \rho}{\partial t} + \vec{\nabla} \cdot (\rho \vec{u}) = 0 \quad (3.0.1)$$

$$\frac{\partial \vec{u}}{\partial t} + \vec{u} \cdot \nabla \vec{u} = -\frac{1}{\rho} \nabla p, \quad (3.0.2)$$

where  $\rho$  is the gas density,  $p$  is the gas pressure,  $\vec{u}$  is the gas velocity and  $t$  is time. We will also assume that  $\rho$  is constant with respect to absolute temperature and is a monotone increasing  $\hat{\rho}$  function of pressure,  $p$ . Let us use the following initial conditions:

$$p = p_0, \quad \rho = \rho_0 = \hat{\rho}(p_0), \quad \vec{u} = 0.$$

Let us assume that  $\tilde{p}$ ,  $\tilde{\rho}$  and  $\vec{\tilde{u}}$  are small disturbances of these initial conditions. In other words,

$$p = p_0 + \tilde{p}, \quad \rho = \rho_0 + \tilde{\rho}, \quad \vec{u} = \vec{\tilde{u}}.$$

Then (3.0.1) and (3.0.2) become

$$\begin{aligned} \frac{\partial \tilde{\rho}}{\partial t} + \vec{\nabla} \cdot [(\rho_0 + \tilde{\rho}) \vec{\tilde{u}}] &= 0 \\ \frac{\partial \vec{\tilde{u}}}{\partial t} + \vec{\tilde{u}} \cdot \nabla \vec{\tilde{u}} &= -\frac{1}{\rho_0 + \tilde{\rho}} \nabla \tilde{p}. \end{aligned}$$

Now, let us recall that the disturbances that we are considering are very small, so their products are negligible. Let us only consider the leading-order terms:

$$\frac{\partial \tilde{\rho}}{\partial t} + \rho_0 \vec{\nabla} \cdot \vec{u} = 0 \quad (3.0.3)$$

$$\frac{\partial \vec{u}}{\partial t} = -\frac{1}{\rho_0} \nabla \tilde{p}. \quad (3.0.4)$$

Let us now use the Taylor expansion, keeping in mind that  $|\tilde{p}| \ll p_0$ ,

$$\begin{aligned} \rho_0 + \tilde{\rho} &= \hat{\rho}(p_0 + \tilde{p}) \\ &\approx \hat{\rho}(p_0) + \tilde{p} \frac{d\hat{\rho}}{dp}(p_0) \\ &= \rho_0 + \tilde{p} \frac{d\hat{\rho}}{dp}(p_0). \end{aligned} \quad (3.0.5)$$

So, at the leading order,

$$\tilde{\rho} = \frac{d\hat{\rho}}{dp}(p_0) \tilde{p}.$$

Hence, (3.0.3) becomes

$$\begin{aligned} 0 &= \frac{\partial}{\partial t} \left( \frac{d\hat{\rho}}{dp}(p_0) \tilde{p} \right) + \rho_0 \vec{\nabla} \cdot \vec{u} \\ &= \frac{d\hat{\rho}}{dp}(p_0) \frac{\partial \tilde{p}}{\partial t} + \rho_0 \vec{\nabla} \cdot \vec{u} \\ -\vec{\nabla} \cdot \vec{u} &= \frac{1}{\rho_0} \frac{d\hat{\rho}}{dp}(p_0) \frac{\partial \tilde{p}}{\partial t}. \end{aligned}$$

Now, let us differentiate with respect to  $t$  and use (3.0.4):

$$-\frac{\partial}{\partial t} [\vec{\nabla} \cdot \vec{u}] = \frac{\partial}{\partial t} \left[ \frac{1}{\rho_0} \frac{d\hat{\rho}}{dp}(p_0) \frac{\partial \tilde{p}}{\partial t} \right]. \quad (3.0.6)$$

Then the right-hand side of (3.0.6) becomes

$$\text{RHS} = \frac{1}{\rho_0} \frac{d\hat{\rho}}{dp}(p_0) \frac{\partial^2 \tilde{p}}{\partial t^2},$$

and the left-hand side of (3.0.6) becomes, using equation (3.0.5),

$$\begin{aligned} \text{LHS} &= -\frac{\partial}{\partial t} [\vec{\nabla} \cdot \vec{u}] \\ &= -\vec{\nabla} \cdot \left( \frac{\partial \vec{u}}{\partial t} \right) \\ &= \frac{1}{\rho_0} \nabla^2 \tilde{p}. \end{aligned}$$

Hence,

$$\nabla^2 \tilde{p} = \frac{1}{c^2} \frac{\partial^2 \tilde{p}}{\partial t^2}, \quad (3.0.7)$$

where we have defined

$$c \triangleq \left( \frac{d\hat{\rho}}{dp}(p_0) \right)^{-\frac{1}{2}}.$$

Equation (3.0.7) is known as the familiar three-dimensional wave equation (Billingham 36).

# Chapter 4

## Solution by Generalized Separation of Variables

After a change of notation, equation (3.0.7) becomes

$$\nabla^2 u = \frac{1}{c^2} \frac{\partial^2 u}{\partial t^2}. \quad (4.0.1)$$

We can rewrite this using Cartesian coordinates as

$$\frac{\partial^2 u}{\partial x^2} + \frac{\partial^2 u}{\partial y^2} + \frac{\partial^2 u}{\partial z^2} = \frac{1}{c^2} \frac{\partial^2 u}{\partial t^2}. \quad (4.0.2)$$

Assume a solution to (4.0.1) of the form

$$u(x, y, z, t) = X(x)Y(y)Z(z)T(t). \quad (4.0.3)$$

Now, substituting (4.0.3) into (4.0.2), we get

$$X''YZT + XY''ZT + XYZ''T = \frac{1}{c^2} XYZT''. \quad (4.0.4)$$

Furthermore, if we divide (4.0.4) by  $u = XYZT$ , we get

$$\frac{X''}{X} + \frac{Y''}{Y} + \frac{Z''}{Z} = \frac{1}{c^2} \frac{T''}{T}. \quad (4.0.5)$$

We now see clearly why this method of separation of variables is so advantageous for this problem. Notice that each additive term of the above equation is a function of only one variable. That is, the first term is only a function of  $x$ , the second of  $y$ , etc. The only way



that this can occur is for each of the terms to be equal to a constant where the constants satisfy (4.0.5).

We shall label the first three separation constants  $-l^2$ ,  $-m^2$ , and  $-n^2$ , respectively. In other words, define

$$\frac{X''}{X} \triangleq -l^2, \quad \frac{Y''}{Y} \triangleq -m^2, \quad \frac{Z''}{Z} \triangleq -n^2. \quad (4.0.6)$$

Now, plugging (4.0.6) into (4.0.5), we see that

$$\frac{1}{c^2} \frac{T''}{T} = -(l^2 + m^2 + n^2) \triangleq -\mu^2.$$

Solving  $X''(x) + l^2X(x) = 0$ , we get

$$X(x) = Ae^{ilx} + Be^{-ilx}.$$

Similarly, we achieve

$$\begin{aligned} Y(y) &= Ce^{imy} + De^{-imy}, \\ Z(z) &= Ee^{inz} + Fe^{-inz}, \\ T(t) &= Ge^{i\mu ct} + He^{-i\mu ct}. \end{aligned}$$

Let us suppose that we take the following as the particular solutions of (4.0.6)

$$\begin{aligned} X(x) &= e^{ilx}, \\ Y(y) &= e^{imy}, \\ Z(z) &= e^{inz}, \\ T(t) &= e^{-i\mu ct}. \end{aligned}$$

Thus, by (4.0.3), we see

$$\begin{aligned} u(x, y, z, t) &= e^{ilx} e^{imy} e^{inz} e^{-i\mu ct} \\ &= \exp[i(lx + my + nz - \mu ct)]. \end{aligned}$$

The above equation represents a plane wave (with unit amplitude) propagating in the  $\vec{k} \triangleq (l, m, n)$  direction with speed  $c$ . Now,

$$\begin{aligned} u(x, y, z, t) &= \exp[i(k_x x + k_y y + k_z z - \omega t)] \\ &= \exp[i(\vec{k} \cdot \vec{r} - \omega t)], \end{aligned}$$

where we have used the common notation for wave theory in which  $\omega \triangleq c\mu$  represents the angular frequency of the wave (Riley 267).

## Chapter 5

# Determining the Modes for a Rectangular Room

Our goal in this section is to solve the **eigenvalue problem**. In other words, we would like to determine the eigenvalues  $k_n^2$  and their corresponding eigenfunctions,  $\Psi_n$ , within the particular solutions of the homogeneous wave equation, which has the form

$$p = \Psi_n(\vec{x})e^{-i\omega_n t}.$$

Here the  $\Psi_n$  satisfy the Helmholtz equation,  $[\nabla^2 + k_n^2]\Psi_n(\vec{x}) = 0$  in  $V$  and the rigid-wall boundary conditions from our rectangular room with volume  $V$  and surface  $S$ ,  $\nabla\Psi_n(\vec{x})\cdot\vec{n}_{out} = 0$  on  $S$ . The boundary conditions come from equation (3.0.4) as the velocity normal to the rigid walls is 0. Basic results from the theory of elliptic partial differential equations tell us that there is a countably infinite sequence of nonnegative real eigenvalues of finite multiplicity for this problem (Renardy and Rogers 303). We call the field associated with a given  $\Psi_n(\vec{x})$  a **room mode**. Let us recall that, for each  $n$ , there is an eigenvalue  $k_n$  which satisfies

$$k_n^2 = \frac{\omega_n^2}{c^2},$$

and that each of the eigenfunctions is a nontrivial solution to the boundary value problem. Our rectangular room will be bounded by rigid walls placed at the planes

- $x = 0, x = L_x$
- $y = 0, y = L_y$
- $z = 0, z = L_z$ .

Let us assume that

$$\Psi_n(\vec{x}) = X(x)Y(y)Z(z)$$

and substitute it into the Helmholtz equation (Pierce 27)

$$\nabla^2 \vec{\Psi}_n + k^2 \vec{\Psi}_n = 0.$$

We get

$$\frac{X''}{X} + \frac{Y''}{Y} + \frac{Z''}{Z} + k^2 = 0.$$

Now, we again know each term is constant. Consider only the first:

$$\begin{aligned} \frac{X''}{X} &= -k_x^2, \\ 0 &= X'' + k_x^2 X, \end{aligned}$$

with boundary conditions

$$\begin{aligned} \frac{\partial \Psi(0)}{\partial x} &= 0, \\ \frac{\partial \Psi(L_x)}{\partial x} &= 0. \end{aligned}$$

So, assuming an equation of the form

$$X(x) = a \cos(k_x x) + b \sin(k_x x),$$

and applying the boundary conditions, we obtain

$$\begin{aligned} X'(x) &= -ak_x \sin(k_x x) + bk_x \cos(k_x x), \\ X'(0) &= \cancel{-ak_x(0)} + bk_x = 0 \quad \implies \quad X = a \cos(k_x x). \end{aligned}$$

Furthermore,

$$\begin{aligned} X'(L_x) &= -ak_x \sin(k_x L_x) = 0, \\ k_x L_x &= n\pi, \\ k_x &= \frac{n\pi}{L_x}. \end{aligned}$$

Hence,

$$X(x) = a \cos\left(\frac{n_x \pi}{L_x} x\right)$$

for some  $n_x \in \mathbb{Z}$ . Similarly, we achieve

$$\begin{aligned} Y(y) &= c \cos\left(\frac{n_y \pi}{L_y} y\right), \\ Z(z) &= d \cos\left(\frac{n_z \pi}{L_z} z\right). \end{aligned}$$

Thus,

$$\Psi = XYZ = A \cos\left(\frac{n_x \pi}{L_x} x\right) \cos\left(\frac{n_y \pi}{L_y} y\right) \cos\left(\frac{n_z \pi}{L_z} z\right),$$

where  $A := acd$ . Now,

$$\begin{aligned} k^2 &= k_x^2 + k_y^2 + k_z^2, \\ k^2 &= \pi^2 \left( \left(\frac{n_x}{L_x}\right)^2 + \left(\frac{n_y}{L_y}\right)^2 + \left(\frac{n_z}{L_z}\right)^2 \right). \end{aligned}$$

Thus, any combination of  $n_x, n_y, n_z$  will produce a mode (Pierce, 284).

## Chapter 6

# The Acoustic Disadvantages of Constructing Rectangular Rooms

Experience teaches us that the shape of a room has an obvious effect on its acoustic properties. For example, many people have compared orating in small rectangular rooms to the undesirable effect of speaking into a small box.

The distribution of resonant frequencies in rectangular rooms are fairly easy to analyze by hand, as we have seen in the previous sections. While many people have provided relative comparisons of different combinations of heights, widths and lengths, an *optimal* room shape has yet to be provided. Circularly-shaped rooms produce very uneven concentrations of sound in certain areas. Cubic rooms have a similar problem in that the three fundamental frequencies and all of their harmonics effectively pile up onto each other.

There was a great deal of inconclusive discussion regarding room ratios in the middle of the last century. In 1942, J.E. Volkmann suggested a 2:3:5 proportion. Shortly thereafter, C.P. Boner claimed that 1:1.26:1.59 ratio would produce the optimum sound. In 1946, R.H. Bolt, considered a vaguely triangularly-shaped area on a length versus width plot (keeping height fixed) of favorable room dimensions (Bolt). In 1965, L.W. Sepmeyer computed statistically three different room dimension ratios. About ten years later, a list of 125 different ratios was put forth by M.M. Loudon. Most of these suggestions fall within the ‘Bolt Area’ (Everest 276-277).

Another unwelcome effect of reflections unrelated to room modes is a “flutter echo,” which is the result of multiple reflections off of hard surfaces. It produces an undesirable ringing effect that occurs after a sharp, percussive sound such as a clapping of a hand (Gervais 17).

Generally speaking, the desired reverberation times for concert halls is significantly greater than that desired for speech and recording studios. Even less than the reverberation times for recording studios are average living rooms (Everest 152-153). We will use this undesirable reflective property to motivate our research in Chapter 7.

## Chapter 7

# The Acoustic and Constructional Advantages of Pentagonal Rooms

Because of effects such as flutter echo, there have been numerous attempts at creating an acoustically optimal room shape by forcing any two opposite boundaries out of their parallelism. The methodology behind it is that, by splaying the walls, one can ‘break up’ some of the degeneracies present in the case of a rectangular room. Up until recently, it was next to impossible to complete any kind of analysis prior to construction of a nonrectangular room. As Everest states, “Making the sound field asymmetrical by splaying walls only introduces unpredictability in listening room and studio situations.” (Everest 282).

Because rectangular rooms have this undesirable reflective property, it would make sense to construct a mixing room with a different geometry – say, that of a pentagon. Hence, the majority of our analysis will be on the regular pentagon. It has a good stereo image (which is symmetric for speaker placement), it is easy to build (as it has few corners) and, unlike the rectangle, prevents early reflections.

# Chapter 8

## Finite Element Methods for Solving the PDE

In this study, COMSOL is used to analyze the eigenvalues of the Laplacian on different shapes.

Using a mesh generator and eigenvalue solver from COMSOL, one is able to input a shape and solve the corresponding eigenvalue problem on that shape. See figures (8.1) to (8.4) for samples of eigenmaps produced by COMSOL.

First, we used COMSOL to see how the eigenvalues calculated from it compared to those that appeared in the Cureton and Kuttler paper (Cureton and Kuttler 90 - 92) for the case of the hexagon with sides of unit length. In particular, this is what we observed:

The color-coding in left-hand column corresponds to eigenvalues that come from various symmetries (see figure 8.6) found in the Cureton and Kuttler paper which used the Schwarz-Christoffel transformation. Here, the eigenvalues coming from the C0 symmetry are black, those from S3 are red, C1 (also S1) are blue, C2 (also S2) are green and C3 are cyan. See Table 8.1.

These discrepancies may be due to the symmetry of the problem. In particular, the Cureton and Kuttler algorithm finds higher multiplicity of the eigenvalues. The symmetry of these is broken by COMSOL.

For the unit-sided pentagon, COMSOL gives us the first sixteen eigenvalues, as can be seen in Table 8.2.

Table 8.1: Comparison of the eigenvalues of the unit-sided hexagon in the Cureton and Kuttler paper with those found using finite-element software.

eigenvalues in paper	eigenvalues calculated using COMSOL
7.1553391146	7.15533945660934
18.1316787	18.1316788513272
	18.1316788606881
32.4518631	32.451860000728
	32.4518600217063
37.4913552	37.4913559195059
47.629373	47.6293735393297
52.678903	52.6378923706469
60.105163	60.1051202520918
	60.1051203073911
70.14046	70.1403756991316
	70.1403757763495
87.53205	87.5319595603236
	87.5319596416963
90.058447	90.0583926762005
94.32577	94.3255820814067
120.86775	
168.82123	
⋮	



Table 8.2: The first sixteen eigenvalues of the unit-sided pentagon found using finite-element software.

10.9964289177312
27.7862076665825
27.7862077786814
49.2736176862388
49.27361825872
57.0945120263032
76.9767357505296
76.9767363518796
89.1672587908845
89.1672598616149
111.119905377419
111.119905874554
126.355586521616
130.131213388052
130.131217367741
147.142102795912

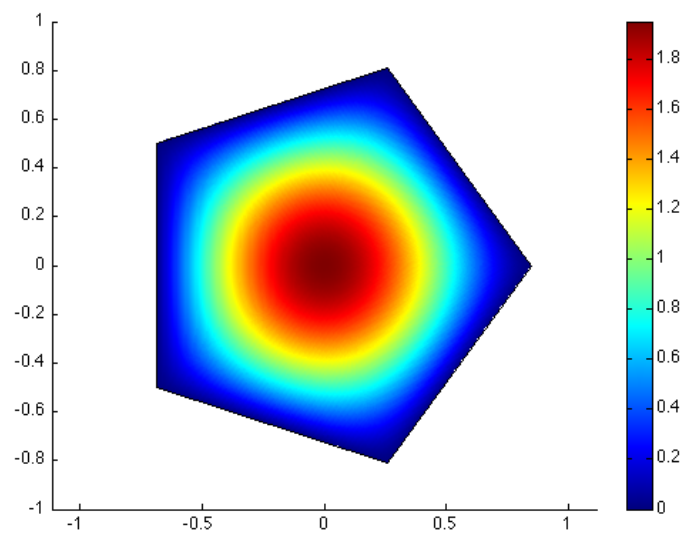


Figure 8.1: The contour map of the eigenfunctions associated with the first eigenvalue in COMSOL.

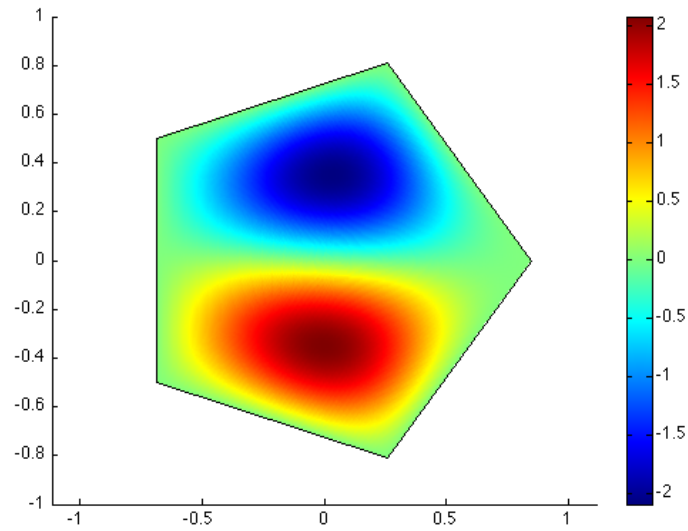


Figure 8.2: The contour map of the eigenfunctions associated with the third eigenvalue in COMSOL.

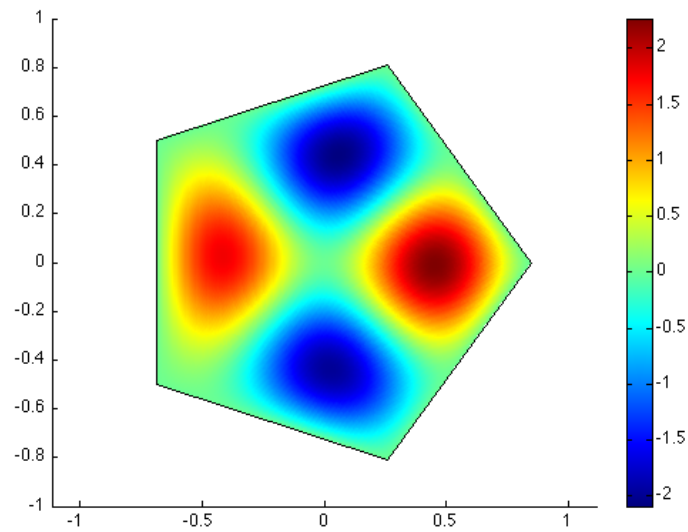


Figure 8.3: The contour map of the eigenfunctions associated with the fifth eigenvalue in COMSOL.

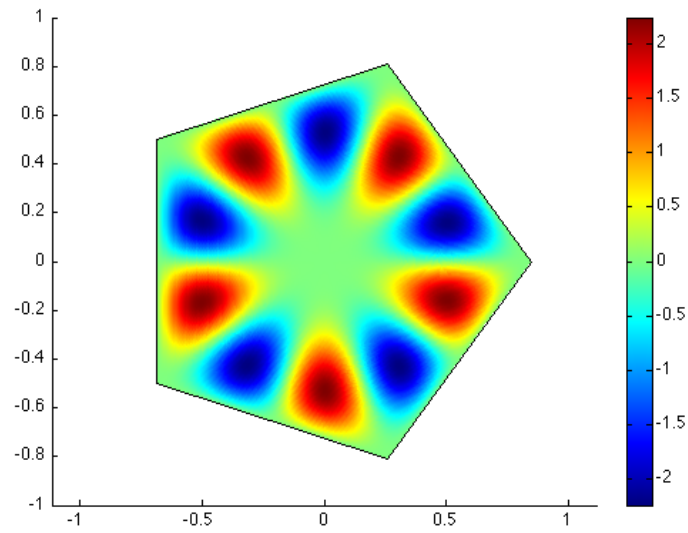


Figure 8.4: The contour map of the eigenfunctions associated with the sixteenth eigenvalue in COMSOL.

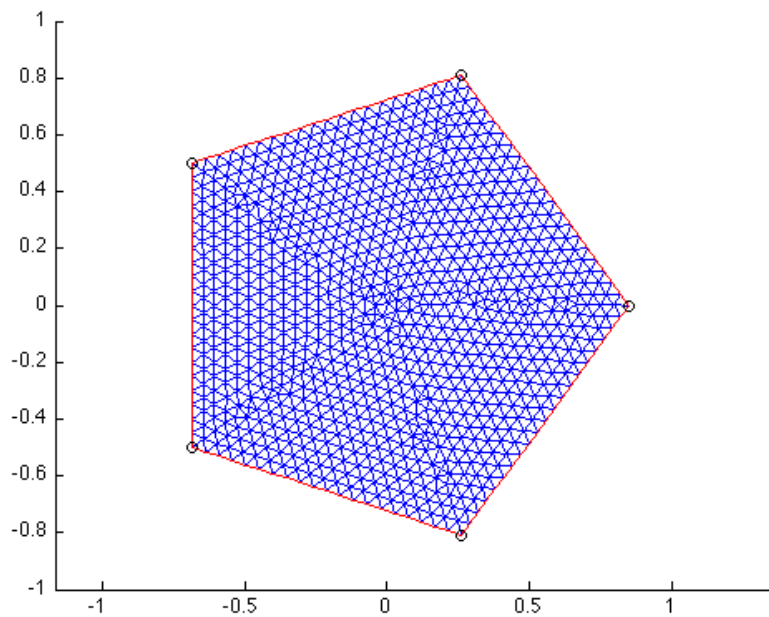


Figure 8.5: Using COMSOL with MATLAB, a triangulated mesh is formulated on the regular pentagon with unit sides.

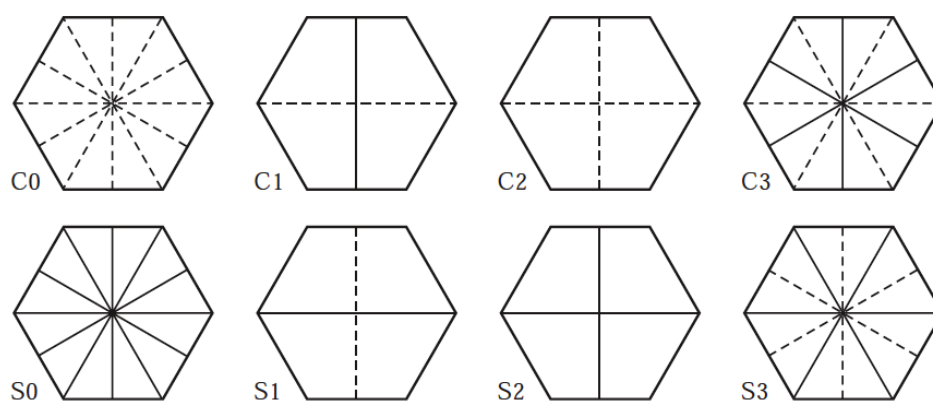


Figure 8.6: The eigenvalues of each of these symmetries were calculated separately in the Cureton and Kuttler paper.

# Chapter 9

## Finding Eigenvalues Using Schwarz-Christoffel Transformations

Thus far, it is clear that the study of eigenvalues of the Laplacian on various geometries is of great importance, especially in the world of acoustics. We have not yet discussed the purpose of this particular method of finding these eigenvalues.

In the last chapter, we examined software designed to handle eigenvalue calculation with ease. With COMSOL Multi-Physics, we need only to input the geometry of the room and a few other parameters, and in moments, the eigenvalues are produced.

However, this is very much a “black-box” method. This thesis attempts to formulate a more analytic method for finding the eigenvalues. Eventually, the hope is to have the ability to vary parameters and optimize the geometry of the room.

### 9.1 Cureton and Kuttler’s Method

In 1998, L. M. Cureton and J. R. Kuttler attempted to solve a similar problem to the one that we have here. They considered the eigenvalue problem for the Laplacian on regular polygons with Dirichlet or Neumann boundary conditions. While they worked out much of the theory in the general case for an  $N$ -sided regular polygon, they only fully worked out an application for the case of  $N = 6$ . In other words, they looked at

$$\Delta\Phi + \lambda\Phi = 0 \quad \text{on } R$$

with Dirichlet conditions

$$\Phi = 0 \quad \text{on } \partial R$$

where  $R$  is the regular hexagon. They use a conformal map to take the unit circle  $C$  in the  $z$ -plane to the regular  $N$ -gon in the  $w$ -plane. Hence, the equivalent problem under the

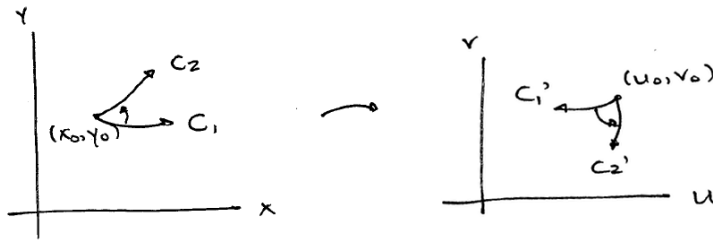


Figure 9.1: Conformal maps preserve angles and sense (direction).

correspondence  $\phi(z) = \phi(w)$  is

$$\Delta\Phi + \lambda\sigma^2\phi = 0$$

on  $C$  where

$$\sigma = \left| \frac{dw}{dz} \right| = |1 - z^N|^{-2/N}.$$

In order to progress further, we must take a deeper look at conformal maps and Schwarz-Christoffel transformations.

## 9.2 Conformal Maps

Suppose we have a set of transformation equations

$$u = u(x, y) \quad \text{and} \quad v = v(x, y).$$

Such a transform is **conformal** at  $(x_0, y_0)$  if it preserves the magnitude and direction of the angle between two curves intersecting at  $(x_0, y_0)$  and  $(u_0, v_0)$  respectively. See Figure 9.1.

Note: A mapping which preserves magnitude, but not sense (direction), is **isogonal**.

The following is a very basic result noting that analytic functions are conformal maps.

**Theorem 9.2.1** *If  $f(z)$  is analytic and  $f'(z) \neq 0$  in a region  $\mathcal{R}$ , then the mapping  $w = f(z)$  is conformal at all points of  $\mathcal{R}$ .*

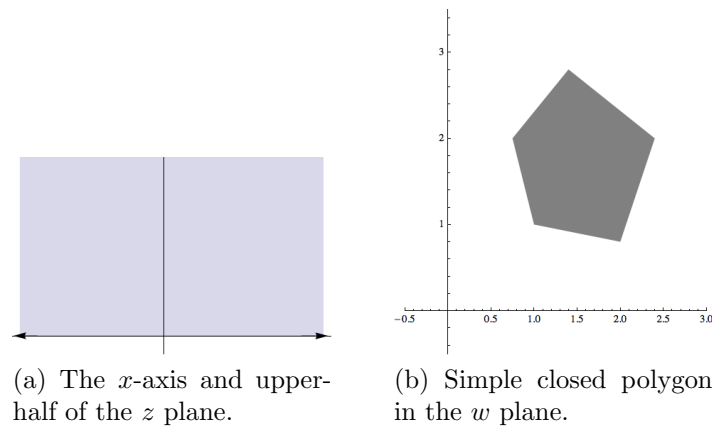


Figure 9.2: The Schwarz-Christoffel Transformation maps the  $x$ -axis to some closed polygon in  $w$ .

### 9.3 Introduction to the Schwarz-Christoffel Transformation

A Schwarz-Christoffel Transformation is an analytic function that maps the  $x$ -axis and upper half of the  $z$ -plane (see Figure 9.2a) onto a given simple closed polygon (see Figure 9.2b).

Suppose we name the vertices of the polygon in the  $w$  plane  $w_1, w_2, \dots, w_n$  with corresponding interior angles  $\alpha_1, \alpha_2, \dots, \alpha_n$  where  $w_i$  maps to  $x_i$  on the real axis of the  $z$  plane.

Such a transformation is given by:

$$\frac{dw}{dz} = A(z - x_1)^{\frac{\alpha_1}{\pi} - 1} (z - x_2)^{\frac{\alpha_2}{\pi} - 1} \dots (z - x_n)^{\frac{\alpha_n}{\pi} - 1}, \quad (9.3.1)$$

or

$$w = A \int_{z_0}^z (s - x_1)^{\frac{\alpha_1}{\pi} - 1} (s - x_2)^{\frac{\alpha_2}{\pi} - 1} \dots (s - x_n)^{\frac{\alpha_n}{\pi} - 1} dz + B, \quad (9.3.2)$$

where  $A, B \in \mathbb{C}$  (Spiegel 204).

**Remark** 1. Any three of the points  $x_1, \dots, x_n$  can be chosen arbitrarily.

2.  $A$  and  $B$  determine the size, orientation and position of the polygon.

3. It is convenient to have, say,  $x_n$  at  $\infty$ .

4. Infinite open polygons can be treated as limiting cases of closed polygons (Spiegel 204).

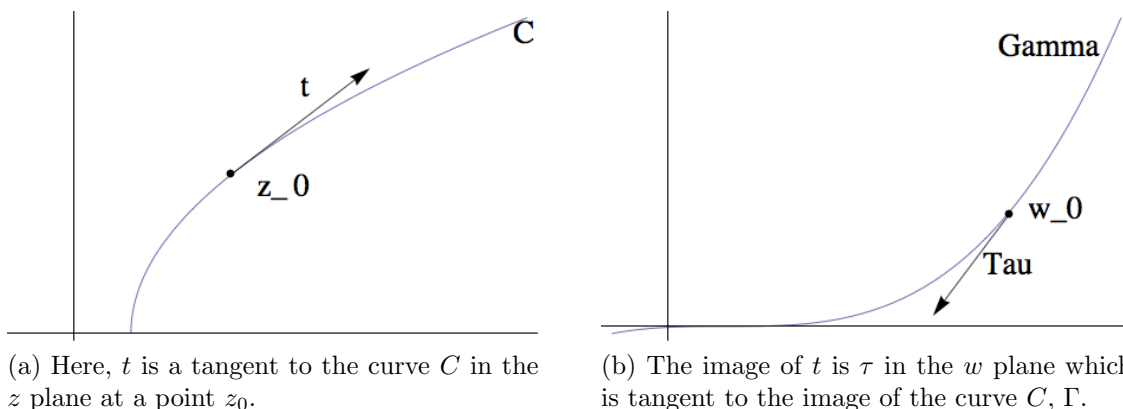


Figure 9.3: The transformation takes the tangent,  $t$ , of the curve  $C$  in the  $z$  plane to the tangent,  $\tau$  of the curve  $\Gamma$  in the  $w$  plane.

Let us establish the validity of the transformation. In other words, let us show that the mapping obtained from (9.3.1) maps the real axis of the  $z$  plane to a given polygon of the  $w$  plane.

Let  $t$  be a tangent to the curve  $C$  at a point  $z_0$  (see Figure 9.3a) and  $\tau$  be the tangent to the image  $\Gamma$  at the corresponding point  $w_0$  under  $w = f(z)$  (see Figure 9.3b).

Assume  $f$  is analytic at  $z_0$  and that  $f'(z_0) \neq 0$ . So

$$\arg \tau = \arg f'(z_0) + \arg t. \quad (9.3.3)$$

In particular, if the curve  $C$  is the  $x$ -axis,

$$t = 1 \implies \arg t = 0$$

at each  $z_0 = x$  on  $C$ . Thus, (9.3.3) simplifies to

$$\arg \tau = \arg f'(z_0).$$

Let us note that if  $\arg f'(z_0)$  is constant, then  $\arg \tau$  is a constant which effectively produces a straight line in  $\Gamma$  (Brown and Churchill 326-327). We now construct a map  $w = f(z)$  that takes the whole  $x$ -axis onto a polygon of  $n$  sides. Denote the points on that axis  $x_1, \dots, x_{n-1}, \infty$ . Their images will be the vertices of the polygon of  $n$  sides and  $x_1 < x_2 < \dots < x_{n-1}$  where the vertices are given by

$$\begin{aligned} w_j &= f(x_j), \quad j = 1, \dots, n-1, \\ w_n &= f(\infty). \end{aligned}$$

We define  $f(z)$  such that  $f'(z)$  jumps from one constant value to another at  $z = x_j$ , as  $z$  traces out the  $x$ -axis:

$$f'(z) = \frac{dw}{dz} = A(z - x_1)^{-k_1} (z - x_2)^{-k_2} \dots (z - x_{n-1})^{-k_{n-1}}$$



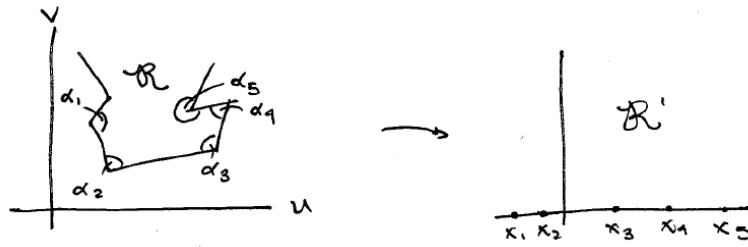
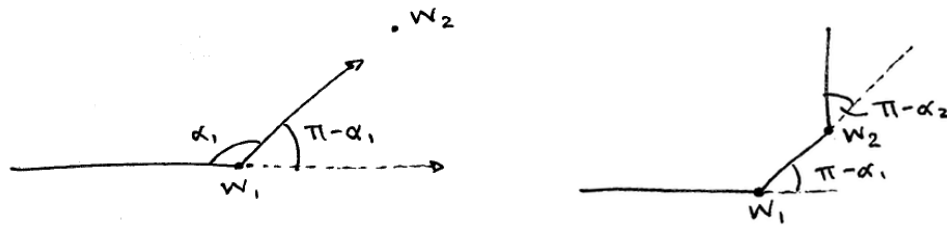


Figure 9.4: As  $z$  traverses the  $x$ -axis, the Schwarz-Christoffel Transformation causes it to make abrupt changes in direction in the  $w$  plane as it passes each  $x_i$  in the  $z$  plane.



(a) As  $z$  crosses  $x_1$ , the image goes through a turn at  $w_1$  of  $\pi - \alpha_1$ .

(b) As  $z$  passes through  $x_2$ , the image makes a turn of  $\pi - \alpha_2$  at  $w_2$ .

Figure 9.5: For each  $x_i$  crossed by  $z$  in the  $z$ -plane, a turn of  $\pi - \alpha_i$  occurs in the  $w$ -plane.

where  $A \in \mathbb{C}$  and  $k_i \in \mathbb{R}$ . Then we get our desired result:

$$\arg dw = \arg dz + \arg A + \left(\frac{\alpha_1}{\pi} - 1\right) \arg(z - x_1) + \left(\frac{\alpha_2}{\pi} - 1\right) \arg(z - x_2) + \dots + \left(\frac{\alpha_n}{\pi} - 1\right) \arg(z - x_n). \tag{9.3.4}$$

Assume as  $x \rightarrow x_1^-$ ,  $w \rightarrow w_1$  along a side of the polygon. When  $z = x$  and  $x < x_1$ ,

$$\arg(z - x_1) = \arg(z - x_2) = \dots = \arg(z - x_{n-1}) = \pi.$$

Then, as  $x$  traverses the  $x$ -axis and  $x_1 < x < x_2$ ,  $\arg(z - x_1) = 0$  and all other arguments remain unchanged at  $\pi$ . Then (9.3.4) implies that  $\arg f'(z)$  jumps up by  $k_1\pi = \pi - \alpha_1$  as  $z$  moves through  $x_1$ . By the same logic, as it moves through  $x_2$ ,  $\arg f'(z)$  jumps up by  $k_2\pi = \pi - \alpha_2$ .

Hence, from (9.3.3), we know that  $\tau$  is constant in direction as  $z$  moves from  $x_i$  to  $x_{i+1}$  on the  $x$ -axis. As  $z$  passes through some  $x_i$ , the direction of  $\tau$  changes abruptly by  $k_i\pi = (\alpha_i - \pi)$ . These angles are the exterior angles of the polygon. See Figure 9.4.

As  $z$  crosses  $x_1$ ,  $\theta_1 = \arg(z - x_1)$  goes from  $\pi \rightarrow 0$  while all of the other terms in (9.3.4) stay

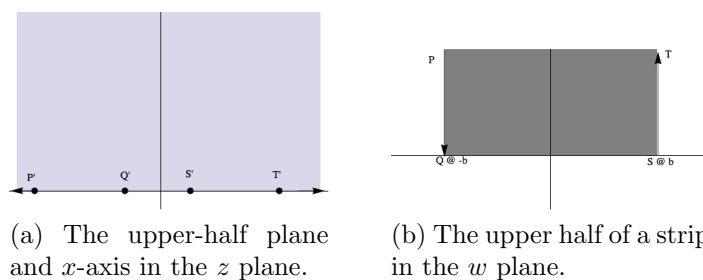


Figure 9.6: We would like to determine a function which takes figure 9.6a to figure 9.6b.

constant. Hence,  $\arg dw$  decreases by

$$\left(\frac{\alpha_1}{\pi} - 1\right) \arg(z - x_1) = + \left(\frac{\alpha_1}{\pi} - 1\right) \pi = \alpha_1 - \pi,$$

or we can think of it as increasing by  $\pi - \alpha_1$ . So the turn at  $w_1$  goes through an angle  $\pi - \alpha_1$ . See Figure 9.5a.

As  $z$  moves through  $x_2$ ,  $\theta_1 = \arg(z - x_1)$  and  $\theta_2 = \arg(z - x_2)$  change from  $\pi \rightarrow 0$ , while all other terms in (9.3.4) stay constant. Hence, another turn of  $\pi - \alpha_2$  is made at  $w_2$ , and so on. See Figure 9.5b.

The following two examples have been adapted from *Schaum's Outline of Theory and Problems of Complex Variables* (Spiegel 220).

**Example** Determine a function which maps Figure 9.6a to 9.6b.

Let  $P, Q, S, T \rightarrow P', Q', S', T'$  respectively. By the Schwarz-Christoffel transformation, since the angles at  $Q$  and  $S$  are equal to  $\pi/2$ , we have, from (9.3.1),

$$\begin{aligned} \frac{dw}{dz} &= A(z+1)^{\frac{\pi/2}{\pi}-1} (z-1)^{\frac{\pi/2}{\pi}-1} \\ &= \frac{A}{(z+1)^{\frac{1}{2}}(z-1)^{\frac{1}{2}}} = \frac{A}{\sqrt{z^2-1}} = \frac{K}{\sqrt{1-z^2}}. \end{aligned}$$

Integrating,

$$w = K \int \frac{dz}{\sqrt{1-z^2}} + B = K \sin^{-1}(z) + B.$$

$$z = 1 \implies w = b \implies b = K \sin^{-1}(1) + B = K \frac{\pi}{2} + B.$$

$$z = -1 \implies w = -b \implies -b = K \sin^{-1}(-1) + B = -K \frac{\pi}{2} + B.$$

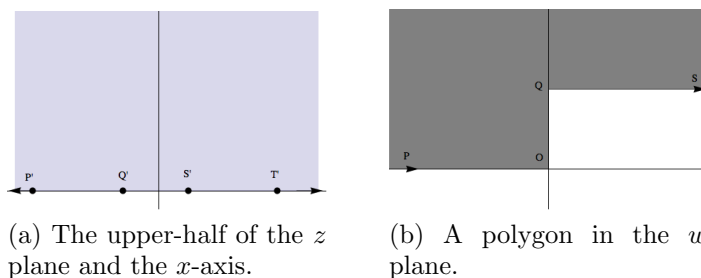


Figure 9.7: We would like to determine a function which takes Figure 9.7a, the upper half plane, to Figure 9.7b, a polygon with right angles.

Hence,  $B = 0$ ,  $K = \frac{2b}{\pi}$  so

$$w = \frac{2b}{\pi} \sin^{-1}(z) \quad \text{or} \quad z = \sin\left(\frac{\pi w}{2b}\right).$$

(Spiegel 220).

**Example** Determine a function which maps Figure 9.7a to 9.7b.

Let  $P, O, Q, S \rightarrow P', O', Q', S'$ . The interior angles of  $O$  and  $Q$  are  $\frac{\pi}{2}$  and  $\frac{3\pi}{2}$  respectively. Equation (9.3.1) implies

$$\begin{aligned} \frac{dw}{dz} &= A(z-0)^{\frac{\pi/2}{\pi}-1} (z-1)^{\frac{3\pi/2}{\pi}-1} \\ &= A\sqrt{\frac{z-1}{z}} = K\sqrt{\frac{1-z}{z}}. \end{aligned}$$

Then

$$w = K \int \sqrt{\frac{1-z}{z}} dz.$$

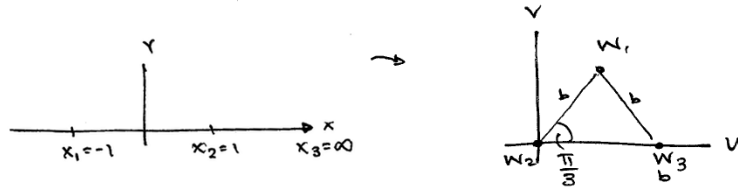


Figure 9.8: Three points on the  $x$ -axis of the  $z$  plane get mapped to an equilateral triangle in the  $w$  plane with side length  $b$ .

Let  $z = \sin^2 \theta \implies dz = 2 \sin \theta \cos \theta d\theta$  to aid in the integration:

$$\begin{aligned}
 w &= K \int \sqrt{\frac{1 - \sin^2 \theta}{\sin^2 \theta}} 2 \sin \theta \cos \theta d\theta \\
 &= K \int \frac{\cos \theta}{\sin \theta} 2 \sin \theta \cos \theta d\theta \\
 &= 2K \int \cos^2 \theta d\theta \\
 &= K \int (1 + \cos 2\theta) d\theta \\
 &= \theta K + \frac{1}{2} K \sin(2\theta) + B \\
 &= K[\theta + \sin \theta \cos \theta] + B \\
 &= K[\sin^{-1} \sqrt{z} + \sqrt{z(1-z)}] + B.
 \end{aligned}$$

Now,

$$z = 0 \implies w = 0 \implies B = 0.$$

$$z = 1 \implies w = bi \implies bi = K \frac{\pi}{2} \implies K = \frac{2bi}{\pi}.$$

Then,

$$w = \frac{2bi}{\pi} (\sin^{-1}(\sqrt{z}) + \sqrt{z(1-z)}).$$

(Spiegel 220).

## 9.4 The Rayleigh-Ritz Method

In order to approximate the eigenvalues of the Laplacian, Cureton and Kutler use the Rayleigh-Ritz Method, which creates upper bounds which approach the real values of the

Table 9.1: The Rayleigh-Ritz array which shows how the method is used to find closer approximations of the eigenvalues.

	1st Problem	2nd Problem	3rd Problem	...	$n$ th Problem	...	Original Problem
1st eigenvalue	$\lambda_1^{(1)} \geq$	$\lambda_1^{(2)} \geq$	$\lambda_1^{(3)} \geq$	$\dots \geq$	$\lambda_1^{(n)} \geq$	$\dots \geq$	$\searrow \lambda_1$
2nd eigenvalue		$\lambda_2^{(2)} \geq$	$\lambda_2^{(3)} \geq$	$\dots \geq$	$\lambda_2^{(n)} \geq$	$\dots \geq$	$\searrow \lambda_2$
3rd eigenvalue			$\lambda_3^{(3)} \geq$	$\dots \geq$	$\lambda_3^{(n)} \geq$	$\dots \geq$	$\searrow \lambda_3$
$\vdots$				$\vdots$			$\vdots$
$n$ th eigenvalue				$\dots \geq$	$\lambda_n^{(n)} \geq$	$\dots \geq$	$\searrow \lambda_n$
							$\vdots$
							$\downarrow$
							$\infty$

eigenvalues as the approximation improves. More particularly, the eigenvalues for the finite dimensional problem act as the upper bounds for those of the infinite-dimensional problem. Thus we have the triangular **Rayleigh-Ritz array** (Gould 66), as displayed in Table 9.1. We should note that **the Rayleigh-Ritz eigenvalues approximate the original eigenvalues from above**.

### 9.4.1 “Intuitive” Explanations of the Rayleigh-Ritz Theorems

Suppose the spectrum of a self-adjoint, nonnegative, compact operator  $K$  is

$$0 < \dots \leq \lambda_n \leq \dots \leq \lambda_2 \leq \lambda_1.$$

Define the **Rayleigh Quotient** (Stakgold 392):

$$R(u) = \frac{\langle Ku, u \rangle}{\|u\|^2} \quad \text{for } \|u\| \neq 0.$$

Let  $M_n = \text{span}\{e_1, e_2, \dots, e_n\}$  where  $\{e_1, e_2, \dots, e_n\}$  are the eigenfunctions of  $K$ .

**Theorem 1.**

$$\max_{u \in M_n^\perp} R(u) = \lambda_{n+1}.$$

We do not know what  $\{e_1, \dots, e_n\}$  are. This time we will use a set of “wrong” functions  $\{v_1, v_2, \dots, v_n\}$  with  $E_n = \text{span}\{v_1, v_2, \dots, v_n\}$ . We will then choose  $E_n$  such that this maximum is minimized. This will lead to the minimax principle.

**Theorem 2.** [Weyl-Courant Minimax Theorem].

Set

$$\nu(E_n) = \max_{u \in E_n^\perp} R(u).$$

Then

$$\lambda_{n+1} = \min_{\text{all choices of } E_n} \nu(E_n).$$

Thus,

$$\lambda_{n+1} = \min_{E_n \in \mathcal{S}_n} \left( \max_{u \in E_n^\perp} R(u) \right),$$

where  $\mathcal{S}_n$  is the set of all  $n$ -dimensional manifolds in  $H$  (Stakgold 393).

### 9.4.2 Rayleigh Quotient in Cureton and Kuttler

In the Cureton-Kuttler paper (Cureton and Kuttler 86), they use a version of the Rayleigh quotient for the modified eigenvalue problem on  $C$  (the unit circle in the  $z$ -plane), given by

$$\frac{D(\phi, \phi)}{\iint_C \sigma^2 \phi^2 dx dy}$$

where

$$D(\phi, \psi) = \iint_C \left( \frac{\partial \phi}{\partial x} \frac{\partial \psi}{\partial x} + \frac{\partial \phi}{\partial y} \frac{\partial \psi}{\partial y} \right).$$

Upper bounds for the eigenvalues are obtained by choosing trial functions  $\phi_1, \phi_2, \dots, \phi_M$  and solving the  $M \times M$  relative matrix eigenproblem

$$[D(\phi_m, \phi_n)] = \mu \left( \iint_C \sigma^2 \phi_m \phi_n dx dy \right). \quad (9.4.1)$$

## 9.5 Calculating the Integrals

The main issue comes in trying to solve the finite dimensional “eigenvalue” problem (9.4.1). This is where the majority of our time spent on the research was done. First, the trial functions  $\phi_n$  used are of the form

$$J_k(j_{k,p}r) \begin{pmatrix} \cos k\theta, \\ \sin k\theta, \end{pmatrix} \quad k = 0, 1, 2, \dots, \quad p = 1, 2, \dots$$

where  $j_{k,p}$  is the  $p$ th root of the  $k$ th Bessel function of the first type,

$$J_k(j_{k,p}) = 0.$$

These are, of course, the eigenfunctions for the “unweighted” eigenvalue problem on the circle. By taking advantage of the orthogonality of the inner product of these trial functions, the integrals on the right-hand side of (9.4.1) become

$$\sum_{n=0}^{\infty} \int_0^1 J_k(j_{k,p}r) J_l(j_{l,q}r) A_n(r) r dr \int_{-\pi}^{\pi} \cos Nn\theta \begin{pmatrix} \cos k\theta \\ \sin k\theta \end{pmatrix} \begin{pmatrix} \cos l\theta \\ \sin l\theta \end{pmatrix} d\theta \quad (9.5.1)$$

where  $A_n(r)$  is defined as

$$\begin{aligned} \sigma^2 &= \sum_{k,l=0}^{\infty} a_k a_l z^{Nk} \bar{z}^{Nl} \\ &= \sum_{k,l=0}^{\infty} a_k a_l r^{N(k+l)} e^{iN\theta(k-l)} \\ &= 2 \sum_{n=0}^{\infty \prime} \cos Nn\theta \sum_{l=0}^{\infty} a_l a_{l+n} r^{N(2l+n)} \\ &= \sum_{n=0}^{\infty} A_n(r) \cos Nn\theta. \end{aligned} \quad (9.5.2)$$

where the prime indicates that the  $n = 0$  has an extra factor of  $\frac{1}{2}$  on it (Cureton 87).

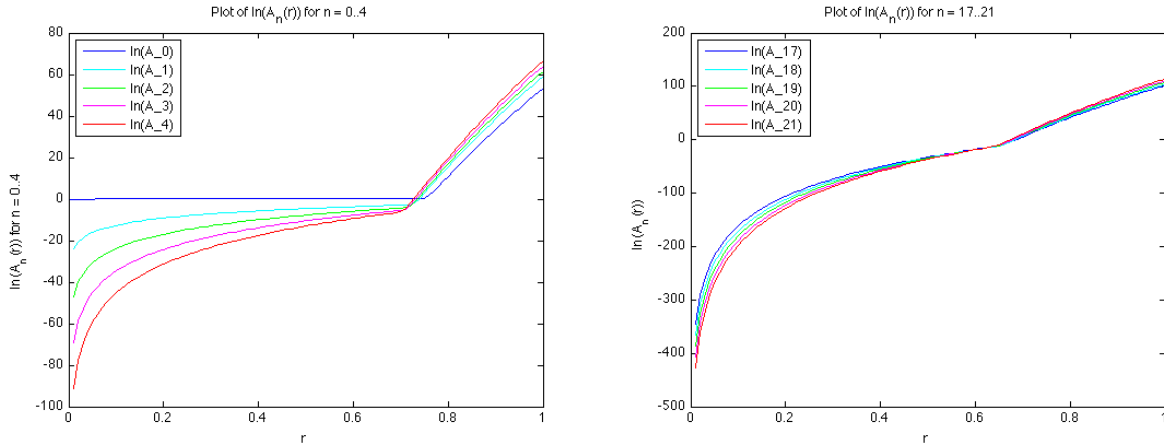


Figure 9.9:  $\ln(A_n(r))$  for  $n = 0, 1, 2, 3, 4$  and  $n = 17, 18, 19, 20, 21$ .

Because of the nature of cosine and sine, only the integrals of cosine with cosine and sine with sine remain. Furthermore, through the use of trigonometric identities, and the fact that  $\int_{-\pi}^{\pi} \cos p\theta d\theta = 0$  unless  $p = 0$ , we see that the integrals vanish unless  $k \equiv \pm l \pmod{N}$ .

Thus, the calculation of the integrals has been reduced to simply evaluating

$$\int_0^1 J_k(j_{k,p}r) J_l(j_{l,q}r) A_n(r) r dr. \quad (9.5.3)$$

Unfortunately, using just Matlab's Quadrature command, the integrals take far too long to evaluate and Cureton and Kuttler claim that it takes more than 4000 terms to achieve "satisfactory precision." This is likely due to the highly oscillatory nature of the Bessel functions. It should also be noted that Mathematica is also incapable of handling these integrals and throws back an error claiming that the integration is converging too slowly. We can see from Figure 9.10 that, as you increase the number of the root of the Bessel function, the function becomes more oscillatory. This makes the direct quadratures much more difficult to accurately calculate.

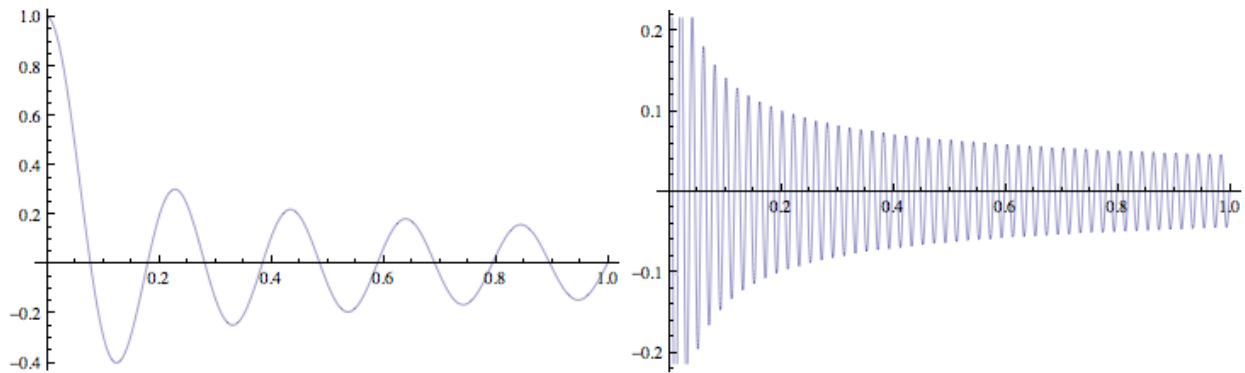


Figure 9.10: The first figure is  $J_0(j_{0,10}r)$  versus  $r$  and the second is  $J_0(j_{0,100}r)$ .

Hence, a recursion formula on  $m$  (for fixed  $k, l, p$  and  $q$ ) was developed (Cureton 88) for integrals of the form

$$I_{00}(m) = \int_0^1 J_k(j_{k,p}r) J_l(j_{l,q}r) r^{m-1} dr. \quad (9.5.4)$$

## 9.6 Calculating $I_{00}$

In order to calculate this integral, using various identities of the Bessel function, one is able to determine that

$$I_{00}(k) = -\frac{1}{k}(I_{10} + I_{01})$$

where

$$I_{10}(k) = \int_0^1 \frac{d}{dx} [J_m(j_{k,p}x)] J_n(j_{l,q}x) x^k dx$$

and

$$I_{01}(k) = \int_0^1 J_m(j_{k,p}x) \frac{d}{dx} [J_n(j_{l,q}x)] x^k dx,$$

as was seen in the paper (Cureton 96-97).



To determine the values of  $I_{10}(k)$  and  $I_{01}(k)$ , we can use the following:

$$\begin{pmatrix} I_{10} \\ I_{01} \end{pmatrix} = \frac{1}{(k^2 - m^2 - n^2)^2 - 4m^2n^2} \begin{pmatrix} k^2 - m^2 - n^2 & 2m^2 \\ 2n^2 & k^2 - m^2 - n^2 \end{pmatrix} \times \begin{pmatrix} \alpha^2 k I_{00}(k+2) - RS \\ \beta^2 k I_{00}(k+2) - RS \end{pmatrix}, \quad (9.6.1)$$

where

$$RS = \beta^2 I_{10}(k+2) + \alpha^2 I_{01}(k+2) + \alpha\beta J'_m(\alpha)J'_n(\beta).$$

In order to calculate the derivatives of the Bessel functions, we used the following identities (Abramowitz 435):

$$\begin{aligned} J_{l+1}(x) &= \frac{l}{x} J_l(x) - J'_l(x), \\ J_{l-1}(x) &= \frac{l+1}{x} J_l(x) + J'_l(x). \end{aligned}$$

Now we can write

$$I_{00}(m) = \int_0^1 J_m(\alpha x) J_n(\beta x) \sum_{k=1}^L p(k) x^{k-1} dx$$

as

$$\int_0^1 J_m(\alpha x) J_n(\beta x) \sum_{k=1}^{k_M-1} p(k) x^{k-1} dx + \sum_{k=k_M}^L p(k) I_{00}(k).$$

Here

$$\begin{aligned} k_M^2 &= \max\left\{m^2 + n^2 + \frac{1}{2}(3\alpha^2 + \beta^2) + \sqrt{4m^2n^2 + \frac{1}{4}(3\alpha^2 + \beta^2)^2 + 2m^2(\alpha^2 + 3\beta^2)}, \right. \\ &\quad \left. m^2 + n^2 + \frac{1}{2}(\alpha^2 + 3\beta^2) + \sqrt{4m^2n^2 + \frac{1}{4}(\alpha^2 + 3\beta^2)^2 + 2m^2(3\alpha^2 + \beta^2)}\right\}, \end{aligned}$$

and  $\alpha = j_{k,p}$  and  $\beta = j_{l,q}$  (Cureton 98).

## 9.7 Implementation of the Method Using $I_{00}$

Cureton and Kuttler claim that using  $I_{00}$  to iteratively calculate (9.5.3) is more efficient than using direct quadrature methods, but do not go into the details of how it is that they actually use this to calculate (9.5.3).

Since the  $n = 0$  case involves a factor of  $\frac{1}{2}$ , we shall first focus on the  $n = 1, 2, \dots$  case. Here, what we see is that, by replacing the  $A_n$  with the definition given in (9.5.2), we achieve the

following expression:

$$\begin{aligned} \int_0^1 J_k(j_{k,p}r)J_l(j_{l,q}r)A_j(r)r \, dr &= \sum_{l=0}^{\infty} 2a_l a_{l+n} \int_0^1 J_k(j_{k,p}r)J_l(j_{l,q}r)r^{2lN+nN+1} \, dr \\ &= \sum_{l=0}^{\infty} 2a_l a_{l+n} I_{00}(2lN + nN + 2). \end{aligned}$$

Here the last line comes from comparing the above expression to the definition of  $I_{00}$  in (9.5.4). For  $n = 0$ , the expression is the same, but without the factor of 2. Therefore,  $m$  is defined as

$$m = 2lN + nN + 2. \quad (9.7.1)$$

Cureton and Kuttler restricted themselves to the case where  $N = 6$ , in other words, hexagons. Hence, their  $m$  was always even:

$$m(\text{mod } 2) \equiv nN = 6n = 0.$$

However, in our case,  $N = 5$  and hence we had to look at both even and odd values of  $m$ . The algorithm was adapted to take this into account.

# Chapter 10

## Results

Originally, we set out to use this method of the Schwarz-Christoffel transformations to obtain the matrix given by the right-hand side of the following equation, found in the Cureton and Kuttler article:

$$\frac{1}{\mu}[D(\phi_m, \phi_n)] = \iint_C \sigma^2 \phi_m \phi_n dx dy \quad (10.0.1)$$

where the trial functions are given by (9.5) and  $\sigma^2$  is defined by (9.5.2). However, we are unable to bring this method to its completion. However, we have taken it nearly all the way.

One of the most important conclusions that we can make with regard to this method is that the iterative implementation of  $I_{00}$  seemed to be an effective way of calculating the integral 10.1.1.

### 10.1 Observations about $I_{00}$

It should first be noted that the reason for calculating  $I_{00}$  is to facilitate the computation of integrals of the form

$$\int_0^1 J_k(j_{k,p}r) J_l(j_{l,q}r) A_n(r) r dr$$

which arise as one attempts to find the eigenvalues of the main problem:

$$[D(\phi_m, \phi_n)] = \mu \left[ \iint_C \sigma^2 \phi_m \phi_n dx dy \right].$$

Since  $A_n(r)$  are simply polynomials in  $r$ , we can further simplify the form of these integrals to

$$\int_0^1 J_m(\alpha x) J_n(\beta x) \sum_{k=1}^L p(k) x^{k-1} dx. \quad (10.1.1)$$

As previously mentioned, the problem with evaluating this in MATLAB using a quadrature is that the function itself is highly oscillatory, due to the nature of the Bessel functions.

Hence, the quadrature should only be used for small values of  $k$ . The algorithm outlined in the previous section for  $I_{00}$  will hence be used for those higher values of  $k$ . Therefore, we create some stopping value  $k_M$  which depends on  $m, n, \alpha$  and  $\beta$  in which we will switch from using the direct quadrature to the algorithm described above.

$$\int_0^1 J_m(\alpha x) J_n(\beta x) \sum_{k=1}^{k_M-1} p(k) x^{k-1} dx + \sum_{k=k_M}^L p(k) I_{00}(k).$$

After several numerical experiments, we see that for various stopping values  $L$ , (or, rather starting values, as the algorithm starts at  $L$  and descends through values of  $k$ ) the algorithm produces the same  $I_{00}$  for values below the lowest  $L$ . In other words, in one experiment, we calculated the values for  $k = l = p = q = 2$ ,  $m = 3$ , with the maximum number of roots of the Bessel functions calculated as 4. We computed the table of  $I_{00}$  for values from  $L = 100$  and lower and for values of  $L = 1000$  and lower. In both tables, by the time that  $I_{00}(80)$  is calculated, the two tables agree to all displayed decimal places.

From this, we are able to assert that, no matter where we begin our calculation of  $I_{00}$ , the algorithm is stable. In addition, in the range of values where we “believe” the quadrature (that is,  $I_{00}$  for low  $m$ ), the computation of  $I_{00}$  by the quadrature agrees to the displayed number of decimal places with the computation of  $I_{00}$  using the algorithm. Hence, our algorithm seems to be in accord with the direct integration of  $I_{00}$ .

Let us consider the case where  $k = p = l = q = 2$ ,  $L = 100$  and the maximum amount of roots of the Bessel function we will include is 32 in the equation

$$I_{00}(m) = \int_0^1 J_k(j_{k,p}r) J_l(j_{l,q}r) r^{m-1} dr.$$

We achieve Table (10.1).

What we see is that, for  $m$  below  $k_M = 17.3031787737509$ , this iterative method agrees with the quadrature, as expected, since the quadrature is “believable” for low values of  $m$ , where the Bessel functions do not oscillate as often.

Thus, we have achieved only partial success in calculating the eigenvalues of the matrix using the method which utilizes Schwarz-Christoffel transformations. We believe, however, that we are one step closer to a more analytic approach to solving this eigenvalue problem.

Table 10.1: A comparison of the calculation of integrals using the iterative  $I_{00}$  algorithm and MATLAB's direct quadrature.

$m$	$I_{00}(m)$ using the iterative algorithm	$I_{00}(m)$ using MATLAB's quadrature
99	0	2.28727076077773e-06
98	1.11065635666416e-05	2.45401335926865e-06
97	1.1454015092114e-05	2.63292307721461e-06
96	1.14704217371668e-05	2.82488956149963e-06
95	1.18295402530734e-05	3.03086779591075e-06
94	1.22149557642492e-05	3.25188294488753e-06
93	1.26058665473745e-05	3.48903556353043e-06
92	1.30131827864325e-05	3.74350720269619e-06
91	1.34385346023413e-05	4.01656644045534e-06
90	1.38825547222355e-05	4.30957537386984e-06
89	1.43462471148313e-05	4.62399660799353e-06
88	1.4830721175282e-05	4.96140078223545e-06
87	1.53371496811867e-05	5.3234746779019e-06
86	1.58667838834801e-05	5.71202995377041e-06
85	1.64209616142487e-05	6.12901256401888e-06
⋮	⋮	⋮
35	0.000204257623479566	0.000208604000880439
34	0.000220805157663154	0.000225014001253417
33	0.000239143973508679	0.000243204380051423
32	0.000259516980429967	0.000259648661187578
31	0.000282206685471018	0.000282347394056461
30	0.000307542731510415	0.000307700922825369
29	0.000335911075505624	0.000336098011337355
28	0.0003677652078735	0.000367995791502638
27	0.000403639923071821	0.000403933752453586
26	0.000444168293127484	0.000444550975155396
25	0.000490102681179272	0.000490607447962328
24	0.00054234087618632	0.000543010533520994
23	0.000601958754071488	0.000602847964280915
22	0.000670251305314342	0.000671429147441576
21	0.000748784459620748	0.000750337095797233
20	0.000839460954056037	0.000841494021092926
19	0.000944604642617966	0.000947244613135997
18	0.00106706931827066	0.00111587965562462
17	0.00121038064109744	0.00121047056776583
16	0.00137892375041897	0.00137899312292838
15	0.00157819578611846	0.00157821790841002
14	0.00181515432981749	0.00181509205918823
13	0.00209871502225623	0.00209852096174029
12	0.00244049622711774	0.00244011630972782
11	0.00285600324323941	0.00285612926611563
10	0.00336665578856509	0.0033668063609367
9	0.0040035566100584	0.00400375534445882
8	0.00481510823289865	0.00481392297775367
7	0.00588368085236523	0.00588274654594424
6	0.00736485098373711	0.0073655902975024
5	0.00958628702250834	0.00958682468406619

# Chapter 11

## Conclusion

It is clear that solving the eigenvalue problem for the Laplacian on various geometries is of great importance to many fields, not the least of which is acoustics. Currently, there are various methods out there that efficiently handle this problem but are evaluated by methods involving finite elements. The goal of this paper was to adapt research already done by Driscoll , Cureton and Kuttler to handle the eigenvalue problem on the pentagon, a room shape which, for various reasons, is often chosen by sound engineers to mix in.

While the methods used up until this point are very “black-box” in nature, they currently seem to provide the best environment for analysis of these problems. This alternate method which uses Schwarz-Christoffel transformations is only partially successful, in that it is clear that the computation times are much longer and they do not facilitate variation in parameters, as was hoped. We are able to take this transformation method to nearly its final stage of completion. Along the way, however, it becomes obvious that this was not the analytic method that we had hoped for. Due to complications involving the Schwarz-Christoffel transformation, the numerics and code quickly become rather abstruse and difficult to interpret. This may be the reason why we were unable to take this method to its completion in finding these eigenvalues. It is possible that we have misinterpreted the original paper put forth by Cureton and Kuttler. Thus, the chances of being able to actually optimize the room shape are rather slim when using this method as it stands right now. The hope is that, in the future, the computational processes will be made more efficient and that this method may eventually become more widely-accepted in the analysis of the spectrum of the Laplacian on various geometries. It may, one day, lead to the optimization (with respect to acoustic properties) of a room shape.

# Bibliography

1. Abramowitz, M., and I. Stegun. *Handbook of Mathematical Functions*. Dover, 1965. Print.
2. Billingham, J., and A. C. King. *Wave Motion: Volume 24 of Cambridge Texts in Applied Mathematics*. Cambridge U P, 2000. Print.
3. Bolt, R. H. "Note on Normal Frequency Statistics for Rectangular Rooms." *J Acoust Soc Am* 17, 101A (1946): 130-133.
4. Brown, James W., and Ruel V. Churchill. *Complex Variables and Applications*. McGraw-Hill, Inc., 1996.
5. Cureton, L. M., and Kuttler, J. R. "Eigenvalues of the Laplacian on Regular Polygons and Polygons Resulting from Their Dissection." *Journal of Sound and Vibration* 220, 1 (1998): 83-98.
6. Driscoll, Tobin A. "Algorithm 756: A MATLAB Toolbox for Schwarz-Christoffel Mapping." *ACM Transactions on Mathematical Software* Vol 22, No 2, (June 1996): 168-186.
7. Everest, F. Alton, and Ken C. Pohlmann. *Master Handbook of Acoustics*. McGraw Hill Professional, 2009. Print.
8. Gervais, Rod. *Home Recording Studio: Built It Like the Pros*. Thomas Course Technology PTR, 2006. Print.
9. Gould, Sydney Henry. *Variational Methods for Eigenvalue Problems: An Introduction to the Methods of Rayleigh, Ritz, Weinstein and Aronszajn*. Courier Dove Publications, 1995. Print.
10. Pierce, Allan D. *Acoustics: An Introduction to Its Physical Principles and Applications*. Acoustical Society of America, 1989. Print.
11. Renardy, Michael, and Robert C. Rogers. *An Introduction to Partial Differential Equations*. Springer 2004. Print.

12. Riley, Kenneth Franklin. *Mathematical Methods for the Physical Sciences: An Informal Treatment for Students of Physics and Engineering*. Cambridge U P, 1974. Print.
13. Spiegel, Murrary R. *Schaum's Outlines of Theory and Problems of Complex Variables*. McGraw-Hill Book Company, 1964. Print.
14. Stakgold, Ivar. *Green's Functions and Boundary Value Problems*. John Wiley & Sons, 1979. Print.